applied nano

MDPI

Article

Binary Biocompatible CNC–Gelatine Hydrogel as 3D Scaffolds Suitable for Cell Culture Adhesion and Growth

Luca Zoia [1], Anna Binda [2], Laura Cipolla [3], Ilaria Rivolta [2] and Barbara La Ferla [3,*]

[1] Department of Earth and Environmental Science, University of Milano-Bicocca, Piazza della Scienza 1, 20126 Milan, Italy; luca.zoia@unimib.it
[2] Department of Medicine and Surgery, University of Milano-Bicocca, Via Cadore 48, 20900 Monza, Italy; anna.binda88@gmail.com (A.B.); ilaria.rivolta@unimib.it (I.R.)
[3] Department of Biotechnology and Biosciences, University of Milano-Bicocca, Piazza della Scienza 2, 20126 Milano, Italy; laura.cipolla@unimib.it
* Correspondence: barbara.laferla@unimib.it; Tel.: +39-0264483421

Abstract: Binary nano-biocomposite 3D scaffolds of cellulose nanocrystals (CNCs)—gelatine were fabricated without using chemical crosslinking additives. Controlled oxidative treatment allowed introducing carboxyl or carbonyl functionalities on the surface of CNCs responsible for the crosslinking of gelatine polymers. The obtained composites were characterized for their physical-chemical properties. Their biocompatibility towards different cell cultures was evaluated through MTT and LDH assays, cellular adhesion and proliferation experiments. Gelatine composites reinforced with carbonyl-modified CNCs showed the most performing swelling/degradation profile and the most promising adhesion and proliferation properties towards cell lines, suggesting their potential application in the field of tissue engineering.

Keywords: 3D-scaffold; gelatine; cellulose nanocrystals; tissue engineering

Citation: Zoia, L.; Binda, A.; Cipolla, L.; Rivolta, I.; La Ferla, B. Binary Biocompatible CNC–Gelatine Hydrogel as 3D Scaffolds Suitable for Cell Culture Adhesion and Growth. *Appl. Nano* **2021**, 2, 118–127. https://doi.org/10.3390/applnano2020010

Academic Editor: Nagendra Kumar Kaushik

Received: 29 April 2021
Accepted: 18 May 2021
Published: 24 May 2021

1. Introduction

Tissue engineering represents a frontier on damaged tissue and organ repair, which are difficult to be addressed by conventional therapeutic interventions [1,2]. Tissue engineering needs an interdisciplinary approach, often relying on biomaterials and scaffolds. Within this framework, on one hand, it is necessary to consider the chemical–physical and mechanic characteristics of the scaffold. On the other hand, it is necessary to evaluate its biocompatibility in terms of lack of toxicity, cellular adhesion and proliferation properties and ability to differentiate into a new tissue [3]. In such a context, the scaffold holds a primary role in the interaction with native tissues. It promotes tissue repair, thus supporting cell adhesion, growth and differentiation and finally, tissue restoration. One of the main components of the extracellular matrix (ECM) is collagen. Therefore, collagen-based materials should represent the best candidates for developing tissue engineering scaffolds, with several examples already reported [4–6]. However, safety concerns, in particular associated with its immunogenicity, have emerged [7]. Gelatine is a natural biopolymer derived from the partial acid or base hydrolysis of collagen. This biopolymer retains most of the principal characteristics of the parental structure, such as biocompatibility, biodegradability, and cellular adhesion properties. Moreover, it is nontoxic and non-immunogenic. However, gelatine has very poor mechanical properties, limiting its application in tissue engineering [8]. Different methods have been adopted to overcome these limitations, among which crosslinking [9–11] and using reinforcing materials were investigated. Among biofillers, cellulose nanocrystals (CNCs) were inserted in the scaffold framework using different approaches. During the last decade, CNCs have been studied for their application in the biomedical field due to their characteristics of biocompatibility [12], large availability, easy surface functionalization [13] and antibacterial properties [14]. As reinforcing material

for gelatine, different approaches have been exploited for generating the scaffold matrix through chemical or physical crosslinking. Feng et al. obtained CNC–gelatine composites by simply mixing solutions of the two components in different ratios and studying their bioprinting properties [15]; Hivechi used glutaraldehyde as a crosslinking agent, produced electrospun CNC–gelatine nanofibers and evaluated its toxicity on cell cultures [16]. Hafizi fabricated a gelatine–CNCs hydrogel using gamma irradiation [17] and investigated its structural properties. Another approach is based on the surface modification of CNCs by introducing aldehyde functionalities that allow forming a crosslinking network through covalent bond formations with amine residues of gelatine without using toxic chemical reagents. In addition, the obtained composite hydrogels showed promising performance in the bioprinting process, fundamental for 3D scaffold generation [18–20]. In the present study, we prepared different gelatine–CNC—-reinforced hydrogels, comparing physical and chemical crosslinking, electrostatic interactions exploiting TEMPO-oxidized CNCs (CNC–COOH) and ammonium ions on gelatine and Schiff base formation through CNCs dialdehydes (CNC–DAD) and amino groups. The obtained hydrogels were characterized for their physical-chemical properties, particularly for their swelling properties, stability in terms of mass loss, biocompatibility, cell adhesion, proliferation and growth using different cell lines.

2. Materials and Methods

Gelatine from porcine skin (type A, Bloom number of 300), Whatman#1 filter paper, 2,2,6,6-tetramethylpiperidine-1-oxyl radical (TEMPO) and sodium periodate ($NaIO_4$), MTT and LDH assay kit were purchased from Sigma-Aldrich. All chemicals were analytical grade and used as received. Deionized water was collected from a Milli-Q purification system of Millipore (USA). Culture dishes, multiwells, DMEM, DMEM/F12, Pen-Strep, L-Glu, FBS, PBS and trypsin for cell culture were purchased from EuroClone.

CNCs preparations. CNCs were extracted from Whatman#1 filter paper by acid hydrolysis according to a previously reported procedure [12] were recovered in about 40% yield, giving a suspension at around 1% *w/v* concentration. The obtained nanocrystals contain on their surface half sulfate esters introduced during the hydrolysis. Therefore, we refer to them also as CNC–SO_3^-.

The obtained CNCs were submitted to TEMPO-mediated oxidation [21,22]. CNC–TEMPO were obtained in 50% yield at a final concentration of 0.5% *w/v*.

CNCs were submitted to $NaIO_4$ oxidation. In particular, in a 250 mL round bottom flask, 100 mL of 1% *w/v* CNCs-SO_3^- (1 g) were added and magnetically stirred. To the CNCs suspension, different amounts of $NaIO_4$ were added (2 or 4 g, 9.3 or 18.6 mmol) at pH 3.5 (adjusted with HCl, 37%). The mixtures were left to react under stirring in the dark at 45 °C for 2 h. At the end of the reaction, 1 mL of ethane-1,2-diol was added. The suspension was purified by dialysis against frequently changed Milli-Q water for 72 h using tubes in cellulose membrane with a molecular weight cut-off of 12,000 Da (Sigma-Aldrich, Milan, Italy). CNC–DA2 and CNC–DA4 (dialdehyde) were recovered with a 50% yield, giving a suspension at around 0.5% *w/v* concentration.

CNCs characterizations. The ATR-FTIR spectra were performed with a Nicolet iS10 spectrometer (Thermo Scientific) equipped with an iTR Smart device (total scan 32, range 4000–800 cm^{-1}, resolution 2 cm^{-1}).

DLS and ζ-potential measurements were performed using a Zeta Sizer Nano 3600 (Malvern) with operating laser (λ = 632.8 nm) and a backscattering angle of 173°. The data were processed by Zetasizer software 7.03. The samples were prepared by diluting initial particles of stock solution to obtain a final concentration of 140 mg/L. Measurements were carried out at 25 °C using a disposable cuvette. Three replicate measurements per sample were performed to establish measurement repeatability.

Hydrogels Preparations. In a 25 mL round-bottomed flask, 1 g of gelatine was dissolved in 10 mL of Milli-Q water under magnetic stirring at 45 °C for 24 h. Then, a suspension of the different CNCs preparations (containing 110 mg of CNCs, 10% concerning the gelatine)

was heated at 45 °C and slowly added to the gelatine solution. The mixture was gently stirred for 15–20 min and poured on glass Petri dishes (diameter 40 mm). The Petri were air-dried for 24 h.

Hydrogel characterizations. A disk of the dried gel (10 mm × 2 mm roughly) was weighed and then rehydrated by immersing in Milli-Q water at 25 °C for 24 and 48 h. After immersion for different times, the specimen was removed from the water. The excess surface water was carefully removed by wiping, and the gel was weighed. The swelling ratio SR (%) was calculated by Equation (1):

$$\text{Swelling ratio SR } (\%) = \frac{\text{Wt} - \text{Wo}}{\text{Wo}} \times 100 \quad (1)$$

where W_o was the initial dried gel weight and W_t was the rehydrated gel weight after 24 or 48 h. All the swelling experiments were done in triplicate. After the swelling experiments, the rehydrated gel was dried by lyophilization and weighed. The mass loss (%) was calculated by Equation (2):

$$\text{Mass loss}(\%) = \frac{\text{Wo} - \text{Wf}}{\text{Wo}} \times 100 \quad (2)$$

where W_o was the initial dried gel weight and W_f was the dried gel weight after 48 h of swelling experiments. The values reported are the means of three analyses with a standard error of ±5%.

SEM analysis. Scanning electron microscopy (SEM) was used to ascertain the morphology and the dimension. The instrument used was a Zeiss Ultra Plus field emission scanning electron microscope operating at 7.0 kV. Samples were prepared by dispersing 10 mL of the suspension in 30 mL of distilled water. The mixture was then sonicated for few minutes. 1 mL of the sonicated suspension was thereafter dispersed in ethanol and sonicated again for about 10 min. About 100 microliters of the sample were deposited on a stub for analysis.

Cell cultures. For the biocompatibility experiments, three different cell lines were used. In particular, L929 is a mouse a fibroblast-like s derived from normal subartaneous areolar and adipose tissue (ATCC); A549 is a human epithelial initiated through explant culture of lung carcinomatous tissue HEK293 (ATCC) and HEK 293, a very common immortalized cell line that, despite its origin is still debated [23], is widely used in cell biology and biotechnology studies. Cells were cultured in DMEM (A549), or DMEM/F12 (L929 and HEK) medium supplemented with 10% fetal bovine serum (FBS), 1% of L-Glutamine and 1% of penicillin/streptomycin and maintained at 37 °C in a humidified CO_2 (5%) atmosphere.

Cell adhesion. Cell adhesion tests were conducted on 60 mm Petri dishes. Three different conditions were identified: either the Petri dishes were treated for cell culture (positive control), or they were suitable for bacterial growing (negative control), or were coated with the selected hydrogel (test condition). 3×10^5 cells were plated and monitored daily for adhesion. Images were taken with a phase-contrast inverted microscope (Leica DMIL) equipped with 10× and 20× objectives.

Cell counting. A simple vital cell counting technique using a Neubauer improved hemocytometer was used to monitor the viability of the cells and their rate of proliferation. Cells were plated at a density of 10^4 cell/well in a 24-wells plate, either treated for cell culture or coated with the selected hydrogels. Each day, three wells for each condition were trypsinized and counted. Trypan blue dye exclusion staining was used for light microscopic quantitation of cell viability. Briefly, after trypsinization, cells were suspended in PBS containing the trypan blue solution at a 1:1 ratio, about 15 µL of the suspension was transferred to the edge of the cell counting chamber and then observed at the light microscope to determine the percentage of viable (unstained) versus the non-viable (stained) cells.

LDH assay. Leaking membranes of damaged or dead cells release the cytoplasmic enzyme lactate dehydrogenase (LDH) into the surrounding medium. Cells were plated in

a 96 multiwell at a density of 2×10^4 cells/well. 24 h after cells seeding, LDH release was analyzed using the cytotoxicity detection kit according to the manufacturer's instruction. The optical density was measured with a microplate reader (Victor3 1420 multilabel counter, PerkinElmer) at 490 nm. The relative amount of released LDH was normalized to the total amount of LDH of control cells, completely lysed with lysis buffer provided from the kit.

MTT assay. Cells were plated in a 96 multiwell at a density of 2×10^4 cells/well. MTT ([3-(4,5-dimetiltiazol-2-yl)-2,5-diphenyltetrazolium bromide]) assay [24] was performed 24 h after cells seeding. Briefly, MTT solution was added to the cells to a final concentration of 0.5 mg/mL. The cells were incubated at 37 °C for 3 h. After incubation, ethanol was added to each well to dissolve the formed formazan crystals. Absorbance at 550 nm was measured with a microplate reader (Victor3 1420 multilabel counter, PerkinElmer). Untreated cells were used as a negative control.

Statistical analysis. All experiments were conducted at least in triplicate independently. Viability values represent the mean of the experiments ± standard deviation (SD). Statistical analyses were performed using OriginPro8 (OriginLab Corporation, Northampton, MA, USA). Data were compared using the unpaired Student's t-test and expressed as means ± SEM (standard error of the mean).

3. Results and Discussion

3.1. CNCs Preparation

To synthesize cellulose nanocrystals from filter paper, selective and controlled hydrolysis in concentrated H_2SO_4 was performed. The conditions permitted the selective acid hydrolysis of the amorphous cellulose regions and the release of the rod-like nanocrystallites in a stable water suspension [25]. This is due to the insertion of sulfate half-esters on the cellulose surface during the extraction procedure. Those samples were named CNC–SO_3^- and characterized by a nanodimension of 155 nm, DPI 0.2. Moreover, the sulfate half-esters (strong acids) on the surface improved the colloidal stability by conferring a ζ-pot equal to −33 mV. SEM image reported in Figure 1 confirmed the rod-like morphology of the nanoparticles and their dimension.

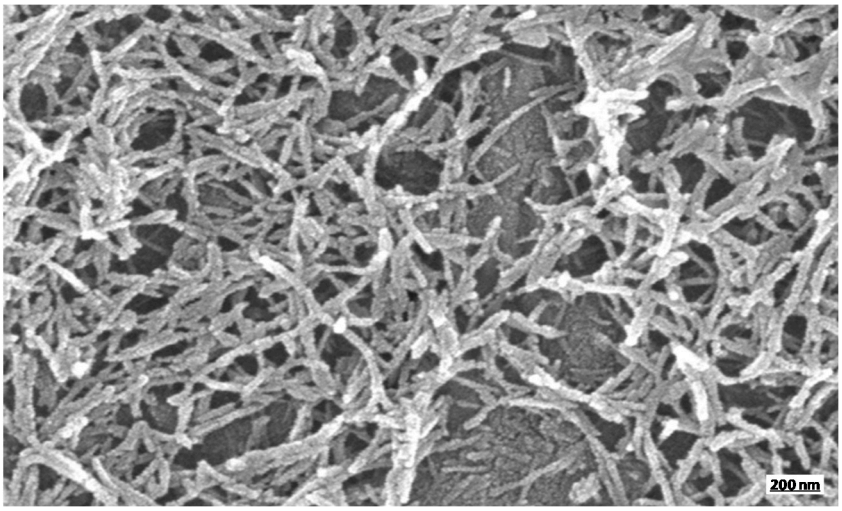

Figure 1. SEM image of CNC–SO_3^-.

Then, the primary hydroxyl groups in C6 on the nanocrystal surfaces were oxidized to carboxylic acids by TEMPO, obtaining CNC–COOH [21,22]. By DLS, the dimension (116 nm, 0.22 DPI) and the ζ-pot (-17 mV) were measured. The oxidation condition slightly decreased the dimension and the ζ-pot, probably by (i) the partial removal of sulfate half-ester due to the required alkaline conditions and (ii) the partial deprotonation of the carboxylic groups (weak acids). Another modification was investigated, the oxidation of the hydroxyl groups in C2 and C3 to aldehydes promoted by $NaIO_4$ [26]. Different oxidant

amounts (2 and 4 g see preparation procedure) were investigated at a constant time (2 h). By DLS, the dimension (74 nm, 0.25 DPI) and the ζ-pot (−20 mV) were measured, indicating that also, in this case, the dimension and the ζ-pot were reduced concerning the starting CNCs. Overall, the ζ-pot measurements indicated that the nanoparticles were synthesized as a stable colloidal suspension (ζ-pot $\leq -20/15$ mV). This evidence could assure a good dispersion of CNCs during the hydrogel preparation avoiding agglomeration and maximizing the reinforcement by polymer–filler interaction. To investigate the surface chemical modifications, FT-IR spectra were acquired. In Figure 2, the spectra of CNC–SO^{3-}, CNC–COOH and CNC–DA (2 and 4 g, 2 h) were overlapped along with the chemical structures of the cellobiose unit. The CNC–SO_3^- spectrum showed the typical bands reported in the literature [27] related to the hydroxyl group that dominated the surface chemistry of those nanoparticles.

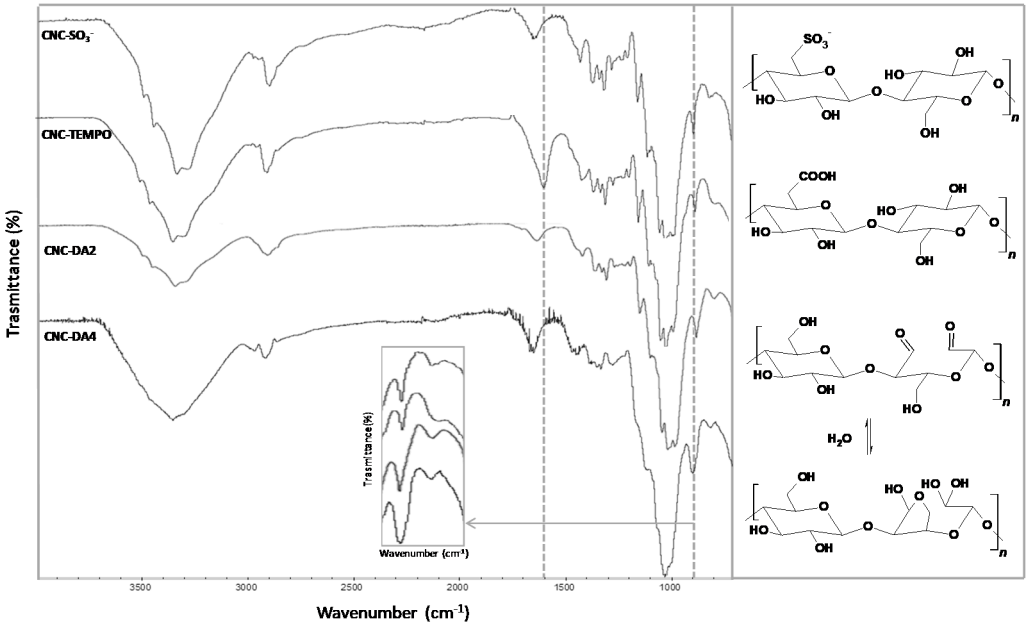

Figure 2. FT-IR spectra of CNC–SO3$^-$, CNC–COOH, CNC–DA2 and CNC–DA4 along with the chemical structures of the representative cellobiose unit.

In particular, the spectrum exhibited the characteristics bands of -OH groups at around 3300 cm^{-1}, of -CH_2- at around 2900 cm^{-1} and of C–O stretching vibrations at 1100–1000 cm^{-1}. After TEMPO oxidation, the carboxylates band at 1600 cm^{-1} was detected as an indicator of oxidation, while, after sodium periodate treatment, the hemiacetals band at around 900 cm^{-1} was detected. Even if this band overlapped with the primary alcohol band of cellulose, it was more significant in FT-IR concerning the expected band of aldehydes at 1700 cm^{-1} after sodium periodate oxidation [28]. This is due to the complex equilibrium, which newly formed aldehydes undergo by intra- and/or intermolecular hemiacetal ring formation. For the sake of clarity, only the hydrated form in C2 and the intramolecular hemiacetal of C3 with the hydroxyl group in C6 are reported. On magnification, it is possible to observe that CNC–DA4 had a stronger absorption than CNC–DA2, indicating that oxidant increasing (from 2 to 4 g) clearly introduced more aldehydes on the nanoparticles. In conclusion, the FT-IR analyses confirmed the surface modifications supporting the conclusion that carboxylic acid and aldehydes were introduced on the CNCs.

3.2. Hydrogels

The different CNC preparations were used at 10% *w/w* to prepare binary hydrogel in the presence of porcine gelatine. The cellulose nanocrystals with sulfate half-esters -SO_3^-, carboxylates -COO^- and aldehydes C=O were investigated as reinforcing filler with

physical/chemical crosslinking ability for the -NH_3^+/-NH_2 groups of gelatine. Sulfate half-esters and carboxylic acids could interact with the amino/ammonium groups of gelatine through ionic interactions. In contrast, the aldehyde groups could react to form imine covalent bonds. FT-IR spectra of pristine gelatine and the different CNC reinforced hydrogels (stack) before and after swelling experiments (overlapped) are reported in Figure 3.

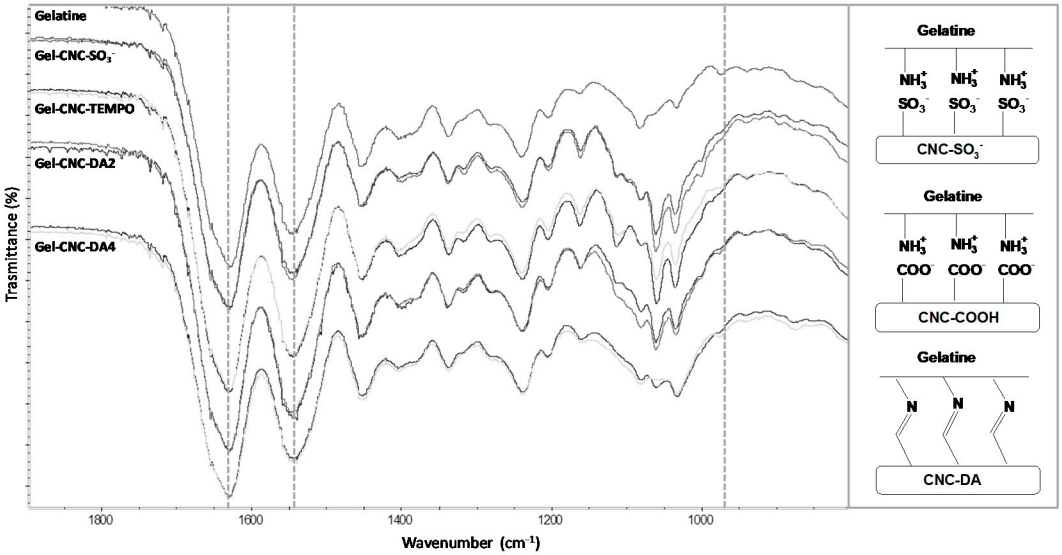

Figure 3. FT-IR spectra of pure gelatine, hydrogel gel–CNC–SO_3^-, gel–CNC–TEMPO and gel–CNC–DA 2 and 4 (stacked) before and after swelling experiments (overlapped) of the different crosslinked composites.

Gelatine characteristic bands at 1630 cm^{-1} (amide I) and at 1530 cm^{-1} (amide II) were easily recognized. Comparison of the gelatine spectrum to the CNC reinforced hydrogels showed a significant difference at around 1000 cm^{-1} in the area of C–O stretching, characteristics of cellulose. The FT-IR spectra of CNC–SO_3^- and CNC–COOH gelatine hydrogel was not able to highlight the ionic interaction, while in the CNC–DA gelatine hydrogel spectra, the reaction of aldehydes and amino groups to form the Schiff's bases was indirectly proved by the disappearing of the acetals band at 900 cm^{-1}. More information was obtained by comparison of the hydrogel spectra before and after swelling experiments (overlapped). It was observed that the characteristic cellulose band (C–O stretching) at around 1000 cm^{-1} changed intensity, and for CNC–SO_3^- and CNC–COOH, we detected a significant increase: this observation was interpreted as a loss of gelatine during the swelling experiments that led to a relative enrichment of CNC in the final hydrogels. For CNC–DA2 and 4, the spectra were almost completely superimposable, indicating that during the swelling experiments, no change in the hydrogel composition occurred. These data are in agreement with hydrogel stability measurements reported in the next section.

3.3. Swelling Behavior and Stability

To investigate the role of CNC surface modifications on the binary hydrogel matrix, swelling and mass loss experiments were performed. The different hydrogel swelling ratios (24 and 48 h) were reported in Figure 4. From the data, it is possible to conclude that the hydrogels reached the swelling balance and higher immersion times (48 h) decreased the swelling ratio for all the samples (except DA4), indicating a partial hydrogel instability. The material solubilized during the test, as observed by FT-IR analyses, was mainly gelatine. The lost gelatine molecules were part of the unbound and/or loosely bound polymeric fraction. This was clear for gelatine alone that was characterized by a high swelling ratio (SR) at 24 h, a strong decrease of SR at 48 h (4000 to 3500%) with roughly 45% as mass loss

(ML). The addition of CNCs strongly decreased the SR (both the absolute value and the difference 24/48 h) and the ML. For CNC–SO^{3-} and CNC–COOH, we measured roughly at SR of 1500% and 600%, respectively, with an ML of around 20% for both the specimens.

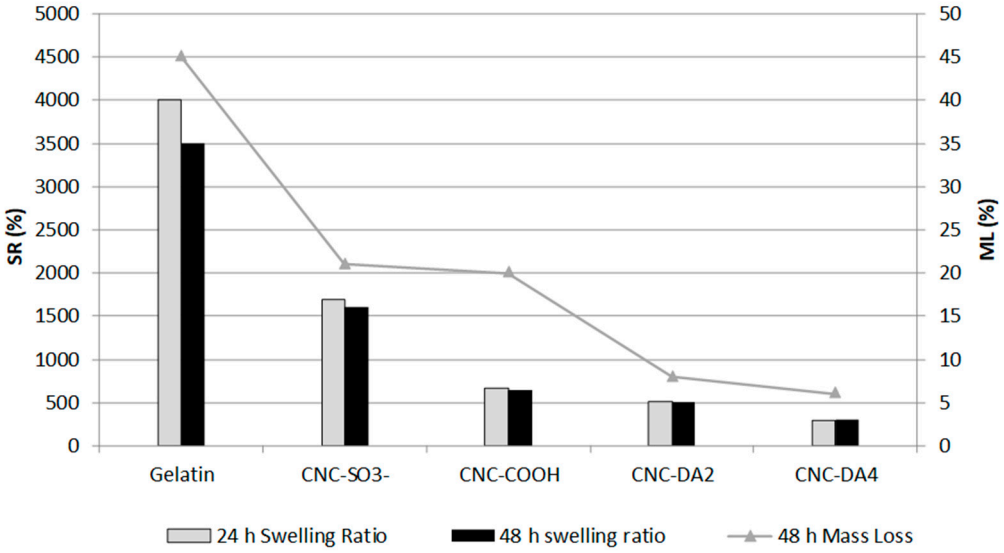

Figure 4. Swelling ratio (SR) at 24 h and 48 h, and mass loss (ML) in% for different hydrogels.

The nanoparticles with sulfate half-ester and carboxylates reinforced the hydrogel increasing the crosslinking and the bound polymeric fraction. Probably the low absolute number of active sites (mainly sulfate half-ester) and their weak ionic interactions (with amines) were not able to create a stable hydrogel. On the contrary, using CNC–DA led to more stable gels with SR at 500 and 300% (respectively 2 and 4 g of oxidant) and an ML under 10%. The imine covalent bonds chemically crosslinked the hydrogels, maintaining gelatine's swelling ability but strongly increasing the stability. Those specimens were considered stable enough and suitable to be explored for cell culture adhesion and growth.

3.4. Cell Adhesion and Growth

The selected hydrogels were submitted to swelling and stability in PBS at 37 °C before cell growth. Adhesion experiments were performed to better simulate physiological conditions. The data for the binary hydrogel gelatine/CNC–DA2 and CNC–DA4 were comparable to those obtained in Milli-Q water. The SR was 630 and 580% for CNC–DAD2 and 380 and 200% for CNC–DAD4 after 24 and 48 h, respectively. The difference 24/48 h was higher, in line with a higher mass loss% for both the specimens, which were finally considered stable on cell growth medium. Since adhesion on supporting substrate is crucial for cell growth, both the selected gelatine hydrogels were tested with L929 and A549 cell lines. Petri dishes treated or not treated for cell culture were positive and negative, respectively (see Methods). After the initial attachment, L929 cultured on CNC–DA2 showed a typical flat and spindle shape. On the contrary, when cultured on CNC–DA4, their shape was rounded and easily detachable. Epithelial cell A549 lose their ability to adhere to the surface on both matrices. We concluded that CNC–DA4 was overall unsuitable for cell growth and discarded it for further studies. CNC–DA2, instead, was also tested on HEK293, which seeded onto such surfaces easily attached and grew (Figure 5).

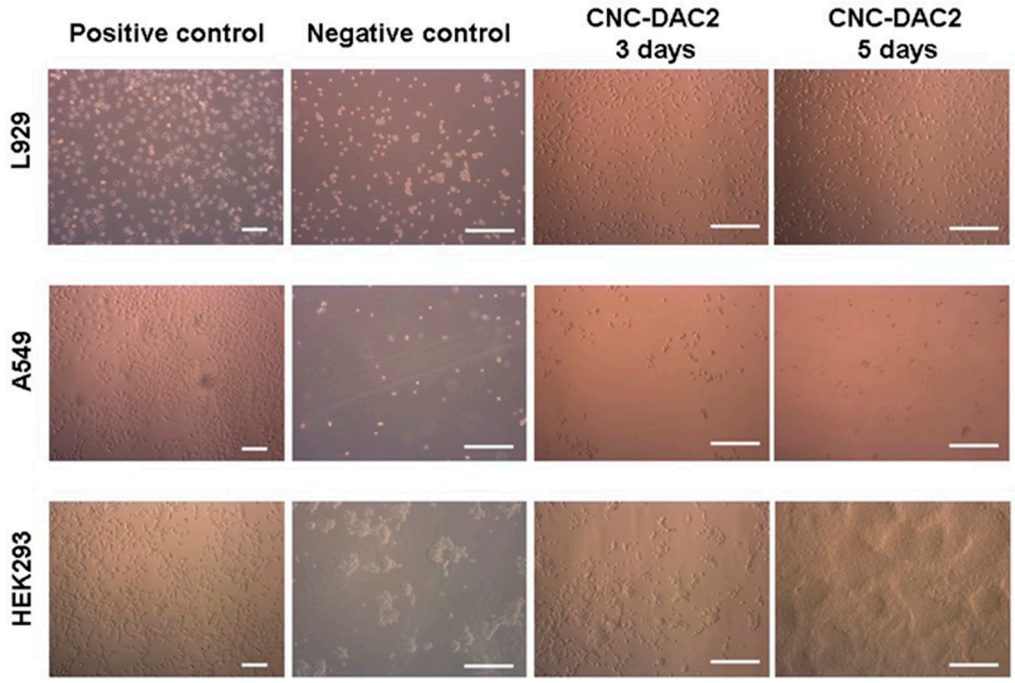

Figure 5. Typical phase-contrast images of the cell lines tested for adhesion to CNC–DAC2 hydrogel gelatine (bright-field, magnification 10× and 20×, the scale bars represent 100 μm) monitored at day 3 and 5 after plating.

Cell attachment occurring in the first stage of cell/matrix interactions may affect cell proliferation. In fact, despite a prolonged lag phase, perhaps due to the cells fitting to the new environment, cells grow evaluation showed increased cell density for both L929 and HEK293 (Figure 6A,B). Detached cells were not detected in the culture medium. Once in the exponential phase, the cell doubling time, measured between the 3rd and 5th day of culture, slowed for the L929, going from about 30 h when growing in the control condition to 48 h when growing on CNC–DA2, and accelerated for the HEK from 48 h when growing in the control condition until about 14 h (insets). To assess the fitness of the cell cultures, the integrity of the plasma membrane (LDH assay) and the metabolic activity (MTT assay) were evaluated. When the cell membrane integrity is compromised, lactate dehydrogenase (LDH), a cytosolic enzyme, is released in the extracellular environment. Thus the presence of this enzyme in the cell culture medium may be considered an index of cell death. As shown in Figure 6C, low levels of LDH were detected. Thus the membrane appears intact in both the cell lines. The level of reducing MTT into formazan by mitochondrial enzymes reflects the level of cell metabolism. This parameter may be considered as a viability index. Both the cell lines considered could convert the MTT into a formazan product. Still, the HEK293 seemed to be slightly more affected by the presence of the hydrogel than L929 (Figure 6D).

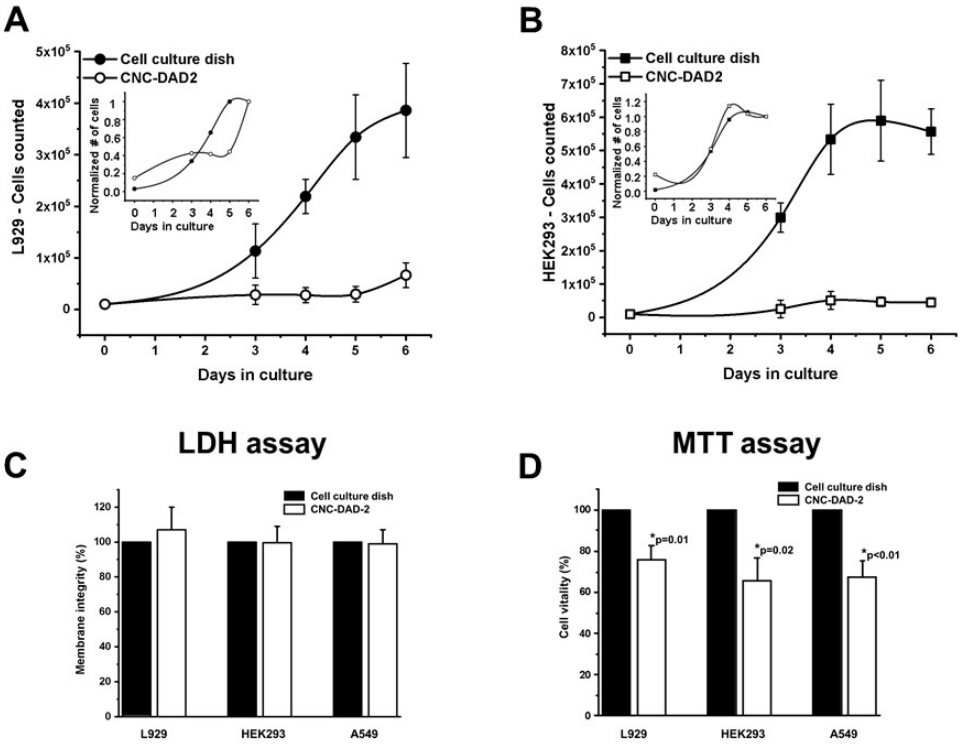

Figure 6. Cell growth and biocompatibility evaluation. (**A**,**B**) Cell growth of L929 and HEK293 cells, respectively, in dishes treated for cell culture and in dishes coated with CNC–DAD2. In the insets, the normalization of the curve to the cell number obtained on the 5th day. (**C**,**D**) LDH and MTT assay, respectively. Data are expressed as means ± standard error of experiments carried out in triplicate.

4. Conclusions

Among the different binary CNC–gelatine biocomposite 3D scaffolds fabricated, the CNC–DAD2 obtained without using crosslinking additives showed the most promising physicochemical characteristics in terms of stability and swelling. The selected scaffold was also biocompatible and nontoxic, as revealed by the MTT assay on all cell lines, and presented very promising adhesion and proliferation properties towards fibroblasts that play a major role in the tissue engineering and regeneration field [24]. These findings pave the way for further development of such scaffold for its possible future application in the field of tissue engineering.

Author Contributions: Conceptualization, B.L.F., L.Z.; methodology, L.Z.; investigation, A.B., L.Z.; resources, B.L.F.; writing—original draft preparation, B.L.F., L.Z., I.R.; writing—review and editing L.C. All authors have read and agreed to the published version of the manuscript.

Funding: This research received no external funding.

Acknowledgments: Chiara Suriano is kindly acknowledged for her enthusiastic work and Heather McFelin for her English editing contribution.

Conflicts of Interest: The authors declare no conflict of interest.

References

1. Sharma, C.; Dinda, A.K.; Mishra, N.C. Fabrication and characterization of natural origin chitosan-gelatin-alginate composite scaffold by foaming method without using surfactant. *J. Appl. Polym. Sci.* **2013**, *127*, 3228–3241. [CrossRef]
2. Zhao, X.; Chen, X.; Yuk, H.; Lin, S.; Liu, X.; Parada, G. Soft Materials by Design: Unconventional Polymer Networks Give Extreme Properties. *Chem. Rev.* **2021**, *121*, 4309–4372. [CrossRef]
3. Ramos, T.; Moroni, L. The Role of Biofabrication—A Year in Review. *Tissue Eng. Regen. Med.* **2019**, *26*, 2.

4. Fagerholm, P.; Lagali, N.S.; Ong, J.A.; Merrett, K.; Jackson, W.B.; Polarek, J.W.; Suuronen, E.J.; Liu, Y.; Brunette, I.; Griffith, M. Stable corneal regeneration four years after implantation of a cell-free recombinant human collagen scaffold. *Biomaterials* **2014**, *35*, 2420–2427. [CrossRef] [PubMed]
5. Jacques, E.; Hosoyama, K.; Biniam, B.; Eren Cimenci, C.; Sedlakova, V.; Steeves, A.J.; Variola, F.; Davis, D.R.; Stewart, D.J.; Suuronen, E.J.; et al. Collagen-Based Microcapsules As Therapeutic Materials for Stem Cell Therapies in Infarcted Myocardium. *ACS Biomater. Sci. Eng.* **2020**, *6*, 4614–4622. [CrossRef]
6. Kilmer, C.E.; Battistoni, C.M.; Cox, A.; Breur, G.J.; Panitch, A.; Liu, J.C. Collagen Type I and II Blend Hydrogel with Autologous Mesenchymal Stem Cells as a Scaffold for Articular Cartilage Defect Repair. *ACS Biomater. Sci. Eng.* **2020**, *6*, 3464–3476. [CrossRef] [PubMed]
7. Stevens, K.R.; Einerson, N.J.; Burmania, J.A.; Kao, W.J. In vivo biocompatibility of gelatin-based hydrogels and interpenetrating networks. *J. Biomater. Sci. Polym. Ed.* **2002**, *13*, 1353. [CrossRef]
8. Liu, X.; Smith, L.A.; Hu, J.; Ma, P.X. Biomimetic nanofibrous gelatin/apatite composite scaffolds for bone tissue engineering. *Biomaterials* **2009**, *30*, 2252–2258. [CrossRef]
9. Gulrez, S.K.; Al-Assaf, S.; Phillips, G.O. Hydrogels: Methods of preparation, characterisation and applications. In *Progress in Molecular and Environmental Bioengineering from Analysis and Modelling to Technology Applications*; InTech: London, UK, 2011.
10. Patel, D.K.; Dutta, S.D.; Shin, W.-C.; Ganguly, K.; Lim, K.-T. Fabrication and characterization of 3D printable nanocellulose-based hydrogels for tissue engineering. *RSC Adv.* **2021**, *11*, 7466–7478. [CrossRef]
11. Yang, C.; Xu, L.; Zhou, Y.; Zhang, X.; Huang, X.; Wang, M.; Han, Y.; Zhai, M.; Wei, S.; Li, J. A green fabrication approach of gelatin/CM-chitosan hybrid hydrogel for wound healing. *Carbohydr. Polym.* **2010**, *82*, 1297–1305. [CrossRef]
12. Colombo, L.; Zoia, L.; Violatto, M.B.; Previdi, S.; Talamini, L.; Sitia, L.; Nicotra, F.; Orlandi, M.; Salmona, M.; Bigini, P.; et al. Organ Distribution and Bone Tropism of Cellulose Nanocrystals in Living Mice. *Biomacromolecules* **2015**, *16*, 2862–2871. [CrossRef]
13. Zoia, L.; Morelli, A.; Talamini, L.; Violatto, M.B.; Lovati, A.B.; Lopa, S.; Recordati, C.; Toffanin, C.; Salanti, A.; Russo, L.; et al. Cellulose Nanocrystals: A multimodal tool to enhance the targeted drug delivery against bone disorders. *Nanomedicine* **2020**, *15*, 2271–2285. [CrossRef] [PubMed]
14. D'Orazio, G.; Munizza, L.; Zampolli, J.; Forcella, M.; Zoia, L.; Fusi, P.; Di Gennaro, P.; La Ferla, B. Cellulose Nano Crystals as Effective Inhibitors of host cell bacteria adhesion. *J. Mater. Chem. B.* **2017**, *5*, 7018–7020. [CrossRef] [PubMed]
15. Feng, C.; Zhou, J.-P.; Xu, X.-D.; Jiang, Y.-N.; Shi, H.-C.; Zhao, G.-Q. Research on 3D bio-printing molding technology of tissue engineering scaffold by nanocellulose/gelatin hydrogel composite. *BioResource* **2019**, *14*, 9244–9257.
16. Hivechi, A.; Bahrami, S.H.; Siegel, R.A. Investigation of morphological, mechanical and biological properties of cellulose nanocrystal reinforced electrospun gelatin nanofibers. *Int. J. Biol. Macromol.* **2019**, *124*, 411–417. [CrossRef] [PubMed]
17. Ishak, W.H.W.; Ahmad, I.; Ramli, S.; Amin, M.C.I.M. Gamma Irradiation-Assisted Synthesis of Cellulose Nanocrystal-Reinforced Gelatin Hydrogels. *Nanomaterials* **2018**, *8*, 749. [CrossRef] [PubMed]
18. Kwak, H.W.; Lee, H.; Park, S.; Lee, M.F.; Jin, H.-J. Chemical and physical reinforcement of hydrophilic gelatin film with dialdehyde nanocellulose. *Int. J. Biol. Macromol.* **2020**, *146*, 332–342. [CrossRef] [PubMed]
19. Jiang, Y.; Zhou, J.; Yang, Z.; Liu, D.; Xv, X.; Zhao, G.; Shi, H.; Zhang, Q. Dialdehyde cellulose nanocrystal/gelatin hydrogel optimized for 3D printing applications. *J. Mater. Sci.* **2018**, *53*, 11883–11900. [CrossRef]
20. Xu, X.; Zhou, J.; Jiang, J.; Zhang, Q.; Shi, H.; Liu, D. 3D printing process of oxidized nanocellulose and gelatin scaffold. *J. Biomater. Sci. Polym. Ed.* **2018**, *29*, 1498–1513. [CrossRef]
21. Saito, T.; Isogai, A. Tempo-mediated oxidation of native cellulose. The effect of oxidation conditions on chemical and crystal structures of the water-insoluble fractions. *Biomacromolecules* **2004**, *5*, 1983–1989. [CrossRef]
22. Huang, C.-F.; Chen, J.-K.; Tsai, T.-Y.; Hsieh, Y.-A.; Andrew Lin, K.-Y. Dual-functionalized cellulose nanofibrils prepared through TEMPO-mediated oxidation and surface-initiated ATRP. *Polymer* **2015**, *72*, 395–405. [CrossRef]
23. Stepanenko, A.A.; Dmitrenko, V.V. HEK293 in cell biology and cancer research: Phenotype, karyotype, tumorigenicity, and stress-induced genome-phenotype evolution. *Gene* **2015**, *569*, 182–190. [CrossRef] [PubMed]
24. Orlando, A.; Re, F.; Sesana, S.; Rivolta, I.; Panariti, A.; Brambilla, D.; Nicolas, J.; Couvreur, P.; Andrieux, K.; Masserini, M.; et al. Effect of nanoparticles binding β-amyloid peptide on nitric oxide production by cultured endothelial cells and macrophages. *Int. J. Nanomed.* **2013**, *8*, 1335–1347.
25. Habibi, Y.; Lucia, L.A.; Rojas, O.J. Cellulose Nanocrystals: Chemistry, Self-Assembly, and Applications. *Chem. Rev.* **2010**, *110*, 3479–3500. [CrossRef] [PubMed]
26. Zhang, L.; Liu, J.; Zheng, X.; Zhang, A.; Zhang, X.; Tang, K. Pullulan dialdehyde crosslinked gelatin hydrogels with high strength for biomedical applications. *Carbohydr. Polym.* **2019**, *216*, 45–53. [CrossRef] [PubMed]
27. Plappert, S.F.; Quraishi, S.; Pircher, N.; Mikkonen, S.K.; Veigel, S.; Klinger, K.M.; Potthast, A.; Rosenau, T.; Liebner, F.W. Transparent, Flexible, and Strong 2,3-Dialdehyde Cellulose Films with High Oxygen Barrier Properties. *Biomacromolecules* **2018**, *19*, 2969–2978. [CrossRef]
28. Wong, T.; McGrath, J.A.; Navsaria, H. The role of fibroblasts in tissue engineering and regeneration. *Br. J. Dermatol.* **2007**, *156*, 1149–1155. [CrossRef]